Experimental determination of frequency- and temperature-dependent electrical properties of water-saturated clays using spectral induced polarization and network analyzer technique

Thierry Bore, Antoine Coperey, Norman Wagner, Partha Narayan Mishra, Alexander Scheuermann, André Revil

▶ **To cite this version:**

Thierry Bore, Antoine Coperey, Norman Wagner, Partha Narayan Mishra, Alexander Scheuermann, et al.. Experimental determination of frequency- and temperature-dependent electrical properties of water-saturated clays using spectral induced polarization and network analyzer technique. Measurement - Journal of the International Measurement Confederation (IMEKO), 2022, 190, pp.110653. ⟨10.1016/j.measurement.2021.110653⟩. ⟨hal-04261881⟩

HAL Id: hal-04261881

https://hal.science/hal-04261881v1

Submitted on 31 Oct 2023

HAL is a multi-disciplinary open access archive for the deposit and dissemination of scientific research documents, whether they are published or not. The documents may come from teaching and research institutions in France or abroad, or from public or private research centers.

L'archive ouverte pluridisciplinaire **HAL**, est destinée au dépôt et à la diffusion de documents scientifiques de niveau recherche, publiés ou non, émanant des établissements d'enseignement et de recherche français ou étrangers, des laboratoires publics ou privés.

HAL Authorization

Measurement 190 (2022) 110653

Contents lists available at ScienceDirect

Measurement

journal homepage: www.elsevier.com/locate/measurement

Experimental determination of frequency- and temperature-dependent electrical properties of water-saturated clays using spectral induced polarization and network analyzer technique

Thierry Bore [a,*], Antoine Coperey [b,1], Norman Wagner [c], Partha Narayan Mishra [a], Alexander Scheuermann [a], André Revil [d]

[a] School of Civil Engineering, University of Queensland, St Lucia, QLD 4072, Australia
[b] University Grenoble Alpes, Univ. Savoie Mont-Blanc, CNRS, UMR CNRS 5204, ISTerre, Le Bourget du Lac, France
[c] Institute of Material Research and Testing, Bauhaus University Weimar, Germany
[d] University Grenoble Alpes, Univ. Savoie Mont-Blanc, CNRS, UMR CNRS 5204, EDYTEM, Le Bourget du Lac, France

ARTICLE INFO

Keywords:
Dielectric spectroscopy
Complex permittivity
Complex conductivity
Clays
Broadband mixture model

ABSTRACT

Impedance and vector network analyzer measurements are combined in order to measure frequency dependent conductivity and permittivity of two different saturated clays: montmorillonite and illite chlorite. In the low frequency range, the complex conductivity is determined over the 10 mHz to 45 kHz frequency range using a complex impedance analyzer with a 4-electrodes cell. In the high frequency range (50 MHz to 5 GHz), the complex permittivity is obtained from measured reflection factor of an open-ended probe. The ultrabroadband constitutive properties of the saturated clays were investigated in the temperature range 25°C down to 0°C. A mixture equation, based on a volume average approach, was applied to model the low and high frequency electrical properties based on the formation factor. The temperature dependency was considered in the following petrophysical quantities: low frequency conductivity, chargeability and high frequency permittivity. The modeled results are in reasonable agreement with measurements.

1. Introduction

Minimal and non-destructive electrical and electromagnetic geophysical techniques have been widely used the past decades in several applications: in hydro geophysics to access ground water resources and quality [1], mining for the characterization of the mine rock waste [2], biogeophysics for dynamic microbial subsurface [3]. The relevant method includes self-potential [4], direct current resistivity [5], frequency or time domain induced polarization [6], ground penetrating radar [7], active or passive microwave remote sensing [8]. However, an ultra-broadband (mHz to GHz) constitutive material model in terms of electrical conductivity, dielectric permittivity and magnetic permeability based on petrophysical properties of geomaterial is not available. The reasons are (i) Maxwells equations allow simplifications for the appropriate field method i.e., operation frequency and hence needed material parameters, and (ii) there is a lack of systematic laboratory investigations over the complete range of frequency for one material. In this study we focus on (ii) and further assume that the material is a lossy dielectric i.e., magnetic permeability is not investigated.

In the low frequency (LF) range below 1 MHz electrochemical impedance spectroscopy (EIS) with two and four electrode cells are used. In geophysical field and laboratory applications the technique used with a four electrode configuration in the mHz to kHz range is called Spectral Induced Polarization (SIP) [9]. The used cells avoid Electrode Polarization (EP) effects [10]. In the kHz to MHz range, the cross talks between electrodes in four electrode configurations leads to difficulties in the proper determination of constitutive electrical material properties. Thus, two electrodes cells are generally used to cover the kHz to MHz range and correct or neglect EP effects [11]. Historically, induced polarization measurements were performed for geophysical prospection of ores. Later it was used in the realm of environmental geophysics to determine textural properties of interest such as

* Corresponding author.
E-mail addresses: t.bore@uq.edu.au (T. Bore), antoine.coperey@gmail.com (A. Coperey), norman.a.wagner@gmail.com (N. Wagner), p.mishra@uq.edu.au (P. Narayan Mishra), a.scheuermann@uq.edu.au (A. Scheuermann), andre.revil@univ-smb.fr (A. Revil).
[1] Now with : Georeva, ZAC du Moulin, 35310 Cintré, France.

https://doi.org/10.1016/j.measurement.2021.110653
Received 29 September 2021; Received in revised form 12 December 2021; Accepted 22 December 2021
Available online 28 December 2021
0263-2241/© 2022 Elsevier Ltd. All rights reserved.

permeability and water content [12,13] or average pore throat parameter [14,15].

In the high frequency (HF) range above 1 MHz the propagation of electromagnetic (EM) waves were used to characterize the complex permittivity of the material. Vector Network Analyzer (VNA) technique in combination with wave guides are used. The electromagnetic characterization of saturated and unsaturated porous geomaterials is carried out with coaxial transmission line cells over the MHz to GHz frequency range [16–18]. For saturated soft soils, the reflection of an EM wave at the open end of a coaxial transmission line in contact to the material have been extensively used [19,20] Based on the seminal work of Topp et al. in time domain [21–23] or Dobson et al. in frequency domain [24], HF-EM measurements have been historically focused on the quantitative in situ determination of soil water content. The coupled electromagnetic, hydraulic and mechanical properties of soils and rocks were investigated decades later based on laboratory characterization of samples under controlled boundary conditions (temperature [25], water content [26], compaction [27]).

It is worth to mention that both measurement methods have rarely been combined. The main reason is probably the difficulty to find a common cell for both methods. The demands on the measuring cell generally differ for each method due to the varying nature of electromagnetic waves with frequency. Another reason is the difficulty to have access simultaneously to both an impedance analyzer and a VNA. As far as the authors know, the first ultra-broadband measurement combining impedance analyser and VNA for soils were done by [28]. Later, several groups have performed such type of measurements but with restricted frequency range, especially in the lower end of the spectrum [29–32]. This limitation in the lower end of the spectrum is a major drawback since important features might not be captured. Otherwise, some alternative methods were proposed by [33] where the electrical properties in frequency domain were computed from Time Domain Reflectometry (TDR) by inverse Fourier transform. Although this method only requires one measurement devices, the frequency bandwidth is considerably reduced: lower limit was around kHz range. As explained earlier, this limitation is a major drawback. Furthermore, the measurement accuracy of the SIP method has greatly improved in recent years [34]. In this context, SIP and coaxial cell transmission line measurements were combined in order to characterize soils (and rocks) over the mHz to 10 GHz range with two different cells [35].

The objectives of this paper are (i) experimental determination and (ii) theoretical prediction of two different petrophysical properties of saturated clays, i.e. electrical conductivity, and dielectric permittivity as a function of frequency and temperature. For this reason, impedance and VNA measurements are combined in order to measure simultaneously broadband low frequency (LF, mHz-kHz) and broadband high frequency (HF, MHz-GHz) electrical properties of two saturated soft clays, montmorillonite and illite chlorite. A four electrodes measurement method was used to measure the complex conductivity in the LF range from 10 mHz to 45 kHz. An open ended (OE) coaxial probe was used to measure the complex permittivity in the HF-range from 50 MHz to 5 GHz. These broadband measurements were combined to investigate the ultra-broadband electrical response of the material as a function of temperature from 25°C down to 0°C (before freezing). An ultra-broadband modeling framework based on the suggested theoretical mixture concept according to [36] is further adapted. The key idea of our approach is that the same formation factor is used to model LF and HF electrical material parameters frequently used in geotechnical and geoenvironmental applications. Against this background, the model is used to predict simultaneously the temperature influence on real high frequency electrical conductivity and real high frequency dielectric permittivity. Moreover, the effect of temperature on the relationship between normalized chargeability and the imaginary part of effective complex conductivity was analyzed.

2. Ultrabroadband electrical properties

2.1. Broadband mixture model

In this study, ferromagnetic materials are not considered, thus magnetic properties can be neglected (e.g. relative magnetic permeability is equal to 1). We also assume time harmonic electrical field vector $\boldsymbol{E} = \boldsymbol{E}_0 \exp(j\omega t)$ with angular frequency ω and imaginary unit j. Based on Maxwell's classical theory of electrodynamics, constitutive broadband electromagnetic material parameters can be equivalently expressed as effective complex conductivity σ^*_{eff} or effective relative complex permittivity $\varepsilon^*_{r,eff}$ [37]:

$$\sigma^*_{eff}(\omega) = j\omega\varepsilon_0\varepsilon^*_{r,eff}(\omega) \tag{1}$$

Based on the ratio of absolute values of current density and conduction current density a loss factor and a critical frequency f_c can be defined (see [25;37] for a detailed description). At frequencies below f_c, σ^*_{eff} is the most effective parameter, and above f_c, $\varepsilon^*_{r,eff}$ is the most effective parameter that determines the general dielectric characteristic of soils and clays.

Geophysical quasi static electrical and wave-based EM techniques are specialized to operate in appropriate frequency bands. Against this background, it is reasonable to define broadband transfer functions as a sum of a low frequency (LF, $<$ 10 kHz) complex conductivity $\sigma^*_{LF}(\omega, T)$ and a high frequency (HF, $>$ 100 MHz) complex relative permittivity $\varepsilon^*_{r,HF}(\omega, T)$ as follows:

$$\sigma^*_{eff}(\omega, T) = \sigma^*_{LF}(\omega, T) + j\omega\varepsilon_0\varepsilon^*_{r,HF}(\omega, T) \tag{2}$$

$$\varepsilon^*_{r,eff}(\omega, T) = \varepsilon^*_{r,HF}(\omega, T) - \mathrm{j}\frac{\sigma^*_{LF}(\omega, T)}{\omega\varepsilon_0} \tag{3}$$

Based on a volume average approach according to Linde et al. (2006) [38], the following expressions including petrophysical properties were introduced to consider LF and HF contributions to the constitutive material properties for fully saturated conditions [36,39]:

$$\sigma^*_{LF}(\omega, T) = \frac{1}{F}\left[\sigma_{DC,W}(T) + (F-1)\sigma^*_S(\omega, T)\right] \tag{4}$$

$$\varepsilon^*_{r,HF}(\omega, T) = \frac{1}{F}\left[\varepsilon^*_{Debye,W}(\omega, T) + (F-1)\varepsilon_g\right] \tag{5}$$

with F the formation factor (dimensionless) which can be related to the (connected) porosity ϕ thanks to the Archie's law: $F = \phi^{-m}$ where m is called the first Archie exponent or cementation exponent [40], $\sigma_{DC,W}$ the real direct current conductivity of the aqueous pore solution, σ^*_S the complex surface conductivity and $\varepsilon^*_{Debye,W}$ the relative permittivity of bulk water according to Debye model. The real direct current conductivity of the aqueous pore solution $\sigma_{DC,W}$ can be computed according to:

$$\sigma_{DC,W}(T) = \sum_{k=1}^{N} \pm z_k e \beta_k(T) C_k \tag{8}$$

with e the charge of an electron, valency $\pm z_k$, ionic mobility in the solution β_k and ionic concentrations in the pore space C_k. The bulk water relative complex permittivity was computed according to Debye model [41]:

$$\varepsilon^*_{Debye,W}(\omega, T) = \varepsilon_\infty(T) + \frac{\varepsilon_{W,S}(T) - \varepsilon_\infty(T)}{1 + j\omega\tau_W(T)} \tag{9}$$

where ε_∞ denotes the high frequency limit of the real part of the relative permittivity, $\varepsilon_{W,S}$ is the quasi static relative permittivity and τ_W is the relaxation time. Above the freezing point, the relaxation time can be computed as a function of temperature according to [42], whereas permittivity at high and low frequencies was computed as a function of

measured temperature according to [43]. The surface conductivity σ_S^* is assumed to be complex because of including the polarization of the Electrical Double Layer (EDL) coating the solid grain (4]. It can be computed according to Cole-Cole model [44]:

$$\sigma_S^*(\omega,T)=\sigma_{\infty,CC}(T)-\frac{\Delta\sigma_{S,CC}(T)}{1+(j\omega\tau_{S,CC}(T))^c} \tag{10}$$

with $\sigma_{\infty,CC}$ is the high frequency (instantaneous) conductivity for the induced polarization process, $\Delta\sigma_{S,CC}$ is the relaxation strength, $\tau_{S,CC}$ the relaxation time and c the stretching coefficient. EDL polarization presents typical relaxation frequencies around tens of Hz [45].

It is worth to note that in the framework of equations (4) and (5), the same formation factor is used to compute LF and HF contributions [36]. Moreover, interfacial processes such as Maxwell Wagner (MW) polarization, and interfacial and confined water relaxation are not considered in our model. MW polarization is induced by charge which accumulate at the boundaries between the different phases with typical frequencies around hundreds of kHz [46,47]. An interfacial water phase exists at lower energy states than that of free water and are physically bound to solid surfaces due to long range van der Waals interactions [48], such that the degree of freedom is different from bulk water in an oscillating electrical field. In this context, it is expected that the relaxation frequency related to interfacial water to be different than bulk water ($\tau_w = 9.60ps$ at T = 20 °C [42], $f_w = 1/(2\pi\tau_w) \approx 16.5GHz$). However, the magnitude of this contribution to the relaxation behaviour of soil under saturated conditions is still under debate [49–51]. Recent research on relaxation behaviour of confined water based on molecular dynamic suggest more complex features such as anisotropy [52] or structure [53]. Please note that in the context of this paper, MW and interfacial or confined water polarization will not be considered. Nevertheless, these processes can be added to the proposed modeling framework. For example, equation (5) was recently extended to integrate interfaces processes by adding Cole-Cole relaxations functions [39,54,55]. In these studies, the developed model was tested and validated in an inverse framework for soil parameters estimation during densification.

Equations (4) and (5) can be extended to cover the whole frequency range:

$$\sigma_{eff}^*(\omega,T)=\frac{1}{F}\left[\sigma_W^*(\omega,T)+(F-1)\sigma_G^*(\omega,T)\right] \tag{11}$$

$$\varepsilon_{r,eff}^*(\omega,T)=\frac{1}{F}\left[\varepsilon_W^*(\omega,T)+(F-1)\varepsilon_G^*(\omega,T)\right] \tag{12}$$

with (i) σ_W^* the broadband complex conductivity and ε_W^* the broadband relative complex permittivity of the aqueous pore solution according to:

$$\sigma_W^*(\omega,T)=\sigma_{DC,W}(T)+j\omega\varepsilon_0\varepsilon_{Debye,W}^*(\omega,T) \tag{13}$$

$$\varepsilon_W^*(\omega,T)=\varepsilon_{Debye,W}^*(\omega,T)-j\frac{\sigma_{DC,W}(T)}{\omega\varepsilon_0} \tag{14}$$

and (ii) σ_G^* the complex conductivity and ε_G^* the complex relative permittivity of a phase including solid particles with a coated/confined aqueous solution as following:

$$\sigma_G^*(\omega,T)=\sigma_S^*(\omega,T)+j\omega\varepsilon_0\varepsilon_g \tag{15}$$

$$\varepsilon_G^*(\omega,T)=\varepsilon_g-\mathrm{j}\frac{\sigma_S^*(\omega,T)}{\omega\varepsilon_0} \tag{16}$$

where ε_g is the real relative permittivity of solid grains which is considered temperature and frequency independent.

2.2. Physico-chemical relations

For geophysical purposes, [36] suggested a simplified model for the high and low frequency conductivity model based on the dynamic Stern layer concept, as:

$$\sigma_\infty(T)=\frac{1}{F}\sigma_{DC,W}(T)+\left(\frac{1}{F\phi}\right)\rho_G B(T).CEC=\frac{1}{F}\sigma_{DC,W}(T)+\sigma_S^\infty \tag{17}$$

$$\sigma_0(T)=\frac{1}{F}\sigma_{DC,W}(T)+\left(\frac{1}{F\phi}\right)\rho_G (B(T)-\lambda(T)).CEC=\frac{1}{F}\sigma_{DC,W}(T)+\sigma_S^0 \tag{18}$$

where CEC is the cation exchange capacity (in $C.kg^{-1}$ but often expressed in $meq/100g$ with $1meq/100g = 963.20C.kg^{-1}$), ρ_G the density of the solid phase (in $kg.m^{-3}$), B (in $m^2.s^{-1}.V^{-1}$) denotes the apparent mobility of the counterions for surface conduction and λ (in $m^2.s^{-1}.V^{-1}$) denotes the apparent mobility of the counterions for the polarization associated with $\sigma_{eff}^{''}$ (or quadrature conductivity). Please note that equation (17) and (18) simply describes the two conduction mechanisms within porous materials. The first term describes the conduction path through the pore-filling electrolyte whereas the second term describes the surface conductivity with the high and low frequency surface conductivity σ_S^∞ and σ_S^0. These equations imply that both paths add in parallel which is conceptually reasonable. B is related to the intrinsic mobility of the counterions in the diffuse layer $\beta_{(+)}$ and the mobility of the counterions in the Stern layer $\beta_{(+)}^S$ by $B=\beta_{(+)}(1-f)+\beta_{(+)}^S f$ with f the partition coefficient (fraction of the counterions of the EDL in the Stern layer); whereas λ is related to the polarization process occurring only in the Stern layer: $\lambda=\beta_{(+)}^S f$. Their temperature dependency (above freezing point) can be expressed with the following equation:

$$B(T)=B(T_0)[1+\alpha_T(T-T_0)] \tag{19}$$

$$\lambda(T)=\lambda(T_0)[1+\alpha_T(T-T_0)] \tag{20}$$

where T_0 and T are the reference temperature ($T_0 = 25^\circ C$) and the temperature in °C and the correction coefficient α_T which denote the sensitivity to temperature for the viscosity of water with typical value around $0.020\ ^\circ C^{-1}$. Same equation with the same coefficient was used to model the temperature dependency of the real direct current conductivity of the aqueous pore solution $\sigma_{DC,W}(T)$.

The normalized chargeability $M_n(T)=\sigma_\infty(T)-\sigma_0(T)$ is defined as:

$$M_n(T)=\left(\frac{1}{F\phi}\right)\rho_G.\lambda(T).CEC \tag{21}$$

A relationship between the normalized chargeability and the quadrature conductivity was developed, which not strictly speaking based on the dynamic Stern layer model, but is helpful in terms of interpretation. If we assume that the real part of the conductivity is not strongly frequency dependent (which is generally the case and it will be confirmed later in that paper – see also Appendix A in [56] for a complete discussion on frequency effect), one can derive liner relationship between the quadrature conductivity measured at the geometric mean of two frequencies f_1 and f_2 and the normalized chargeability defined as the difference between the in-phase conductivity at frequency $f_2 > f_1$ and the in-phase conductivity at the frequency f_1:

$$\sigma_{eff}^{''}\left(\sqrt{f_1 f_2}\right)\approx\frac{M_n(f_1,f_2)}{\alpha}=-\frac{\sigma_{eff}^{'}(f_2)-\sigma_{eff}^{'}(f_1)}{\alpha} \tag{22}$$

with α a constant.

Finally, an approximation was used to compute the real part of the relative effective permittivity at high frequency ε_{HF}:

$$\varepsilon_{HF}=Re(\varepsilon_{r,eff}^*(\omega,T))\approx\frac{1}{F}\left[Re\left(\varepsilon_{Debye,W}^*(\omega,T)\right)+(F-1)\varepsilon_g(\rho_G)\right] \tag{23}$$

where the relative permittivity ε_g of the solid particles is computed as a

function of the density of the solid phase ρ_G according to the empirical model proposed in [24]:

$$\varepsilon_g(\rho_G) = \left(1.01 + 0.44\rho_G.10^{-3}\right)^2 - 0.0062 \quad (24)$$

In general, a frequency of 1 GHz can be used to match with remote sensing method such as Time Domain Reflectometry (TDR) [57] or L-band remote sensing [8].

3. Materials and methods

3.1. Materials

In this study, 2 natural clays were investigated: montmorillonite and illite-chlorite. Sample preparation was carried out in three steps. First, samples were dried at least for 24 h at about 50 °C. Then, samples were saturated by a saline solution under vacuum. The salt solution was prepared just before saturation and consists to a degassed distilled water with a specified weight of salt in order to obtain the targeted conductivity. After the saturation, the saturated samples were left during a week in order to reach equilibrium. For more detail about this procedure see [58]. Before broadband measurement, the supernatant fluid was collected to measure water conductivity. The porosity was determined by volumetric method (using the mass and volume of saturated sample). The CEC was measured by cobalt hexamine chloride method [59]. This method consists to measure the amount of cobalt ion adsorbed on the surface of the grains by colorimetric titration.

The formation factor F (and surface conductivity σ_S) were determined by measuring the real part of low frequency electrical conductivities $\sigma'_{eff}(f \approx 1Hz)$ at different salinity. A sample from the same batch for each material was led to the following salinity: $0.01, 0.1, 1.0, 2.0, 5.0, 10.0 S/m$. The change of salinity is done by diffusion by placing the sample in a large volume of water of the desired salinity (renew regularly to accelerate the equilibrium) and conducted from low to high salinity. The sample is left for several weeks (even more than a month) in the new solution to reach equilibrium. The conductivity of the supernatant fluid is measured regularly, the equilibrium is reached when a stable value is obtained.

Equation (17) and (18) can be written as a linear model: the effective conductivity depends linearly of the conductivity of the aqueous phase. Moreover, if we assume that the real part of the effective complex conductivity in the LF range is slightly frequency dependent, we can write:

$$Re\left(\sigma^*_{eff}\right) \approx \frac{1}{F}\sigma_W + \sigma_S \quad (25)$$

In the previous equation, in order to simplify the notation, σ_S stands for the real part of the complex surface conductivity σ^*_S. This equation was fitted to the bulk conductivity and pore water conductivity curve in a log–log space using a non-linear fitting procedure based on a least square technique. The results are presented on Fig. 1 for the montmorillonite sample. For illite-chlorite sample, the estimation of formation factor was presented in [60].

The values for B ($Na^+, T_0 = 25°C$) and λ ($Na^+, T_0 = 25°C$) from [61] were used. Finally, the complete petrophysical properties of the two samples are summarized in Table 1.

3.2. Method

In the LF range, the effective complex conductivity was measured with the 4 electrodes method and a high precision impedance analyzer build by Zimmerman (ZEL-SIP04-V02) [34]. Resistance and phase shift are measured in the frequency range of 10 mHz to 45 kHz. The device has been benchmarked by comparison with other impedance analyzer [58] and the performance has been characterized by different sensitivity studies: precision on phase shift is $\approx 0.1 - 0.2 mrad$ below 1 kHz.

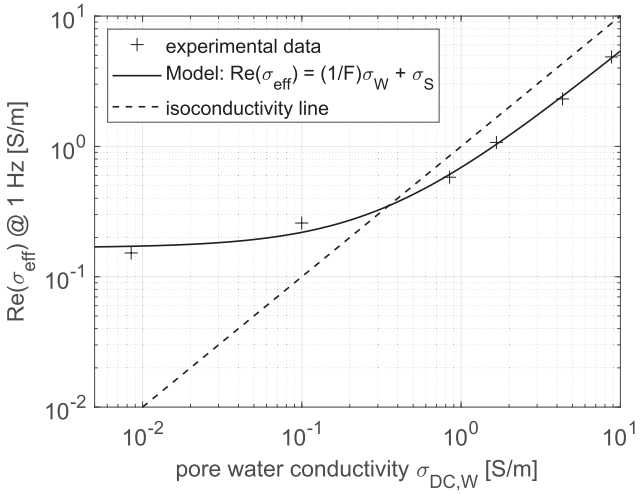

Fig. 1. Determination of the formation factor and surface conductivity for the montmorillonite sample with multi-salinity measurements.

Table 1
Petrophysical parameters of the clay samples.

	Montmorillonite	Illite-chlorite
grain density [$kg.m^{-3}$]	2350	2750
porosity [-]	0.9	0.65
Cation Exchange Capacity CEC [$meq/100\ g$]	41.9	8.6
formation factor F [-]	1.91	2.08
surface conductivity σ_S [S/m]	0.17	0.02
pore water conductivity $\sigma_{DC,W}$ [S/m] @$T = 25\ ^\circ C$	0.52	0.35
apparent mobility B [$m^2.s^{-1}.V^{-1}$] @$T = 25\ ^\circ C$	$3.1.10^{-9}$	
apparent mobility λ [$m^2.s^{-1}.V^{-1}$] @$T = 25\ ^\circ C$	3.10^{-10}	

Moreover, different researchers have been performed a large set of measurement on different type of porous materials (suspensions [62], rocks [63], soils [64]) the last decade with such analyzer. A cylindrical sample holder was used: a plastic cylinder whose diameter is $2.5cm$ and height is $9cm$. The current electrodes A and B are placed at the end faces of the tube, whereas potential electrodes M and N are placed on the surface of the tube and separated by a distance of $5cm$ approximately (see Fig. 1.a). Medical film carbons electrodes were used for the electrodes. Preliminary tests were made to ensure their reliability over time with temperature changes. The effective complex conductivity is computed from the measured complex impedance $Z(\omega)$:

$$\sigma^*_{eff}(\omega) = K\frac{Re(Z(\omega))}{|Z(\omega)|^2} - jK\frac{Im(Z(\omega))}{|Z(\omega)|^2} \quad (26)$$

with K the geometrical factor (in m^{-1}). This factor can be determined by the means of 3D FEM (Finite Elements Method) modeling or with analytical formula. In our configuration, it can be computed with the following relationship: $K = L/A$ where A is the surface of the current electrodes and L is the distance between the two potential electrodes.

In the HF range, the effective relative complex permittivity was measured with a semi rigid open ended probe (SROE) over the 1 MHz to 5 GHz range. The probe consists simply of a semi rigid coaxial line, whose tip has been cut with an angle of 45°. It was simply designed from a RG402 semi rigid coaxial cable (inner diameter: $d_1 = 0.91$ mm, insulator diameter: $d_2 = 2.97$ mm). The sensitive area is the tip which is inserted in the material to be characterized. Based on the two-capacitance model, the following bilinear equation can be derived:

$$\varepsilon^*_{r,eff}(\omega) = \frac{c_1(\omega)S_{11}(\omega) - c_2(\omega)}{c_3(\omega) - S_{11}(\omega)} \quad (27)$$

with $S_{11}(\omega)$ the measured scattering function (reflection only) and $c_1(\omega), c_2(\omega), c_3(\omega)$ the frequency dependent calibration functions. [65] proposed two methods of calibration which are based on measurement of standard whose dielectric properties are perfectly known. The first one, called Open Water Short (OWS), is based on air, deionized water and short measurements. The second one, called Open Water Liquid (OWL), is based on air, deionized water and another reference liquid. A sensitivity analysis on the effect of calibration was performed experimentally and numerically. Results have shown that combining both method for conductive material is the best option. Nevertheless, the study has shown some limitations. Such type of probe could not deliver good complex effective permittivity estimation in the 1 MHz – 50 MHz range due to the lack of sensitivity in this range. Moreover, due to the inaccuracy of short measurement above 500 MHz, it is recommended to use OWS for the 50 MHz – 500 MHz and to use OWL above. The dielectric properties of deionized water were computed as a function of temperature thanks to Debye model. For OWL, methanol was used as extra liquid. The extensive data base of [66] was used to compute the dielectric properties as a function of temperature. Please note that OE probe has been extensively used for soils and rocks application the last decades. The authors have been using this methodology for different soil type: suspensions [67] or clayey soft soils [68].

It is worth to note that the electrical effective parameters were not measured on the same sample. Indeed, the spatial sensitivity of each measurement is quite different. For the LF sample holder, the whole material within the cylinder is investigated whereas for the HF measurement only the region at the close vicinity of the probe is investigated. In this context, for each material two types of sample holder were used.

3.3. Experiment set-up

The different sample holders were put in a bag and immersed in a thermally controlled bath (Kiss K6 from Buber). The temperature of the bath is regulated with a precision of 0.1 °C and the heat carrying fluid in the tank is monoethylene glycol. LF sample holders were put in a sealed bag before being immersed in the bath. For HF measurement, laboratory tests were used a sample holder. The SROE probe was inserted thanks to a hole in the test tube so as the tip of the probe is in contact with the material within the tube. The test tubes, before being inserted in the bath, were sealed with rubber to avoid leaks (Fig. 2).

The ultrabroadband electrical properties were investigated in the temperature range + 25 °C down to 0 °C (before freezing). HF samples and bath were monitored with varnish thermocouples connected to a data logger CR1000 from Campbell scientific. Temperature probes were not inserted in the LF sample holders so as not to disturb the impedance measurements. 7 steps of temperature were made during the decrease of temperature (25 °C, 20 °C, 15 °C, 10 °C, 5 °C, 2 °C and 0°C). For each step, we let enough time for the sample temperature to stabilize. Measurements were performed on different time scale during the experiments. In the HF range, a 2 ports VNA (Keysight E5071C) measuring over the 50 MHz – 5 GHz range was used to measure simultaneously the two clays sample (with 2 probes: one on each port). Measurements were done in monitoring mode: a measurement was done approximatively every 8 min. E5071C was remotely controlled with Python. In the LF range, ZEL-SIP04-V02 was used to measure the complex impedance over the 10 mHz to 45 kHz. Please note that the acquisition of a complete spectrum takes approximately 20 min. Thus, LF measurement were only performed at the end of each temperature step. We manually switch between the 2 samples holder.

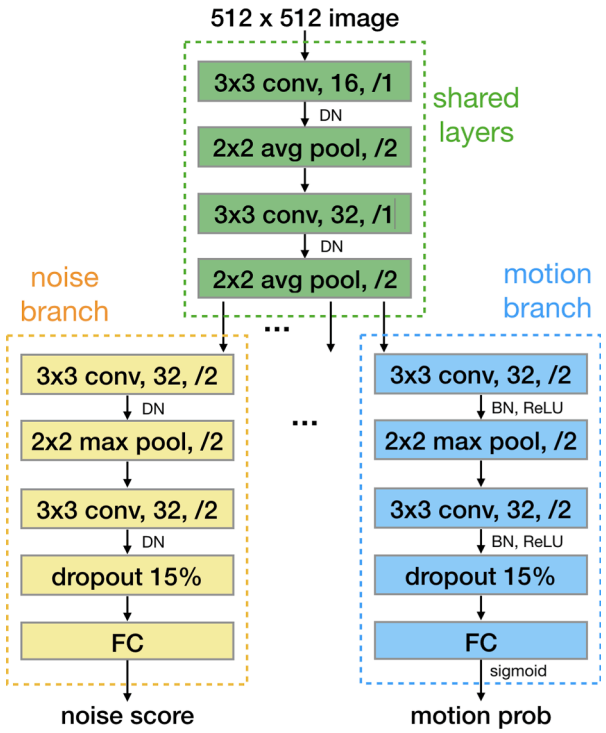

Fig. 2. Equipment and sample holders. a) Thermostat bath with SROE probes inserted in laboratory test tubes. b) Position of sample holders and thermo couples within the bath. c) Sample holder for SIP measurements: A,B currents electrodes; M,N: potential electrodes . d) SROE probes.

4. Results and discussions

Fig. 3 displays the frequency dependent complex conductivity and effective complex permittivity for the montmorillonite sample as a function of temperature. Similar quantities are displayed on Fig. 4 for illite-chlorite sample. In the case of effective relative permittivity an inset has been added to represent only the high frequency data (due to the dynamic of the whole spectrums high frequency data are over-scaled).

The first comment concerns the continuity between low and high frequency measurements. For example, the real part of $\sigma^*_{eff}(\omega)$ shows a good continuity in the case of illite-chlorite whereas in the case of montmorillonite a little offset can be observed. The slight possible difference between the samples (2 samples from the same batch are used) might be the origin of this offset. Otherwise, as expected, the real part of LF complex conductivity is slightly frequency dependent.

Although the investigation of relaxation behavior is not the main objective of this study, one can clearly observe different relaxations processes all over the frequency range. Firstly, in the high frequency region (above 1 GHz), the imaginary part of $\varepsilon^*_{r,eff}(\omega)$ shows the typical signature of free water relaxation. Nevertheless, due to the restricted frequency range of investigation, only the tail of the process can be observed. As expected [42], the relaxation frequency increasing with temperature (e.g. on the inset it can be observed that the tail of the relaxation is shifting to higher frequency when temperature increases). The low frequency part should be dominated by two relaxation processes: EDL relaxation on the lower end and MW relaxation. In the case of illite-chlorite, this can clearly be observed on the imaginary part of $\sigma^*_{eff}(\omega)$ (or on the real part of $\varepsilon^*_{r,eff}(\omega)$). Finally, one can guess an extra process which could be attributed to confined water relaxation in the case of montmorillonite. A closer look on the inset shows a dispersion around hundreds of MHz. This dispersion is very small in the case of illite chlorite. It is expected that a swelling clay such as montmorillonite

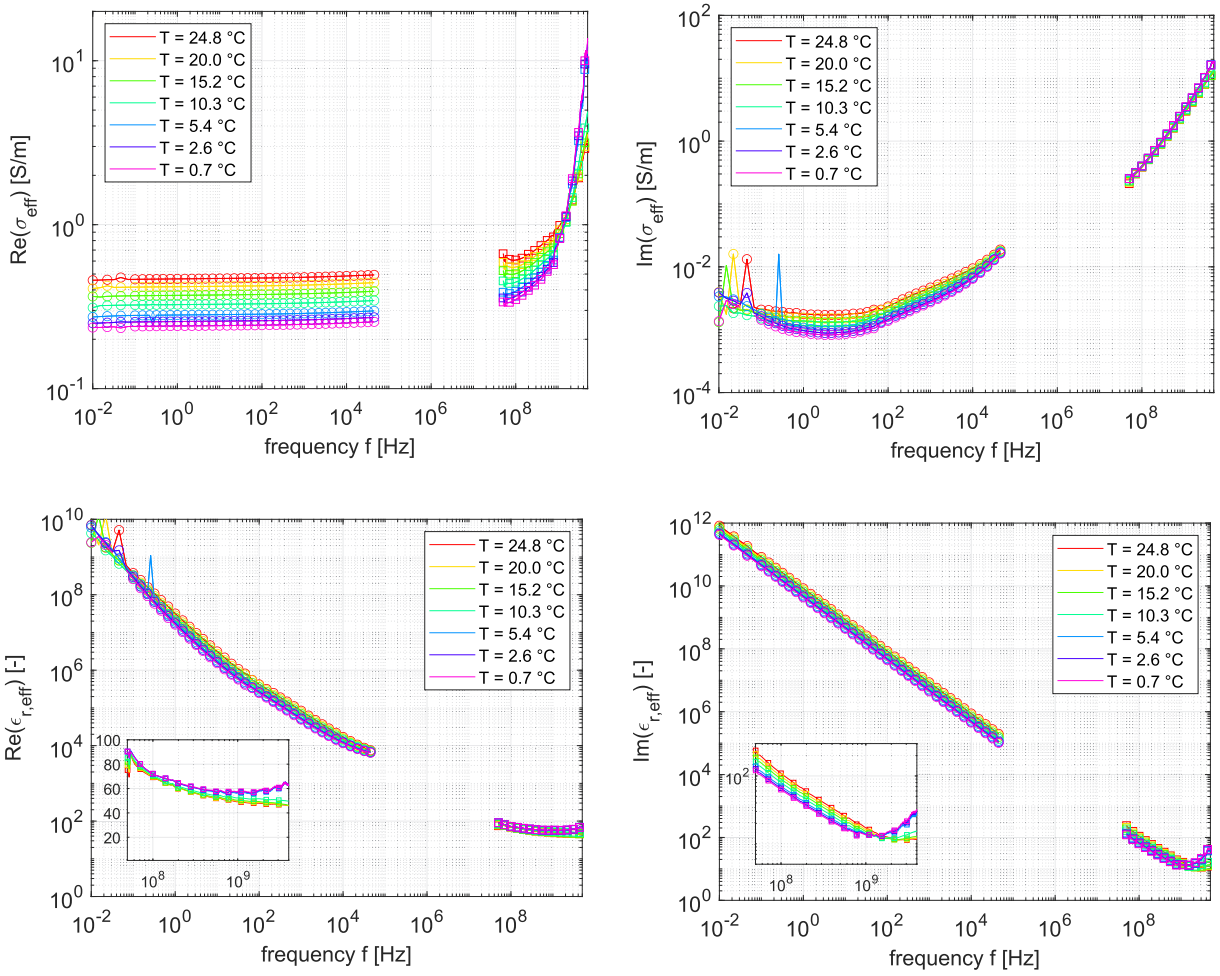

Fig. 3. Ultrabroadband measured spectrums of Montmorillonite, complex conductivity (top, left : real part, right. imaginary part) or complex permittivity (bottom, left. real part, right. imaginary part). LF data with circle marker, HF data with square marker.

presents an important amount of confined water. Nevertheless, measurements in the intermediate would be required to develop a quantitative analysis. A further analysis will be focused on the relaxation behavior; the phenomenological approach suggested in [35] will be used.

The effect of temperature can be observed on the real part of $\sigma^*_{eff}(\omega)$ at low frequency: the conductivity increases with increasing temperature. The effect of temperature can also be observed on the real part of $\varepsilon^*_{r,eff}(\omega)$ at high frequency: the relative permittivity decreases with increasing temperature. These changes will be quantified based on the broadband mixture model in the next step of the paper.

In Fig. 5, the high frequency conductivity σ_∞ as a function of temperature is represented respectively for montmorillonite and illite-chlorite. Values were computed based on equations (17) and (19). The experimental data at $f = 10^4 Hz$ were used. In Fig. 6, the computed values of σ_∞ were plotted versus the measured values at $f = 10^4 Hz$ for both sample for all measurements. The quality of the estimation can be illustrated by the high values of R^2 coefficient.

The relationship between normalized chargeability M_n and the quadrature conductivity is illustrated on Fig. 7 for the complete set of measurements. M_n was defined as the difference of the in-phase conductivity between $f = 10^3 Hz$ and $f = 10^{-1} Hz$, and the quadrature conductivity at the geometric mean frequency ($f = 10^1 Hz$) was used. A good correlation was observed over the whole temperature range ($R^2 = 0.9736$). The constant α can be estimated according to [56]:

$$\alpha \approx \frac{2}{\pi}\ln(10^A) \tag{28}$$

with A the number of decades separating high and low frequency (here A = 4). A theoretical value of 5.86 was obtained, whereas an experimental value of 5.13 was obtained. In other words, the quadrature conductivity can be considered as a proxy for the normalized chargeability (and vice versa). Thus, there is a relationship between the observables measured in time and spectral domains which is temperature independent and true for both materials.

The real part of effective relative complex permittivity at 1 GHz was then computed as a function of temperature based on equation (5), 6 and 7 and the same formation factor used for the analysis of low frequency properties. The results for montmorillonite and illite-chlorite are presented on Fig. 8. Finally, the computed values were plotted versus the estimated values on Fig. 9.

5. Conclusions

In this paper, ultrabroadband electrical properties of two saturated clays, montmorillonite and illite-chlorite, were investigated in the temperature range 25°C down to 0°C (above the freezing temperature of these materials). Low frequency measurements (1 mHz – 45 kHz) were measured with a combination of impedance analyzer and 4 points electrodes, whereas high frequency measurements were performed with a combination of OE probes and VNA. Electrical properties were expressed in terms of effective complex permittivity or effective complex

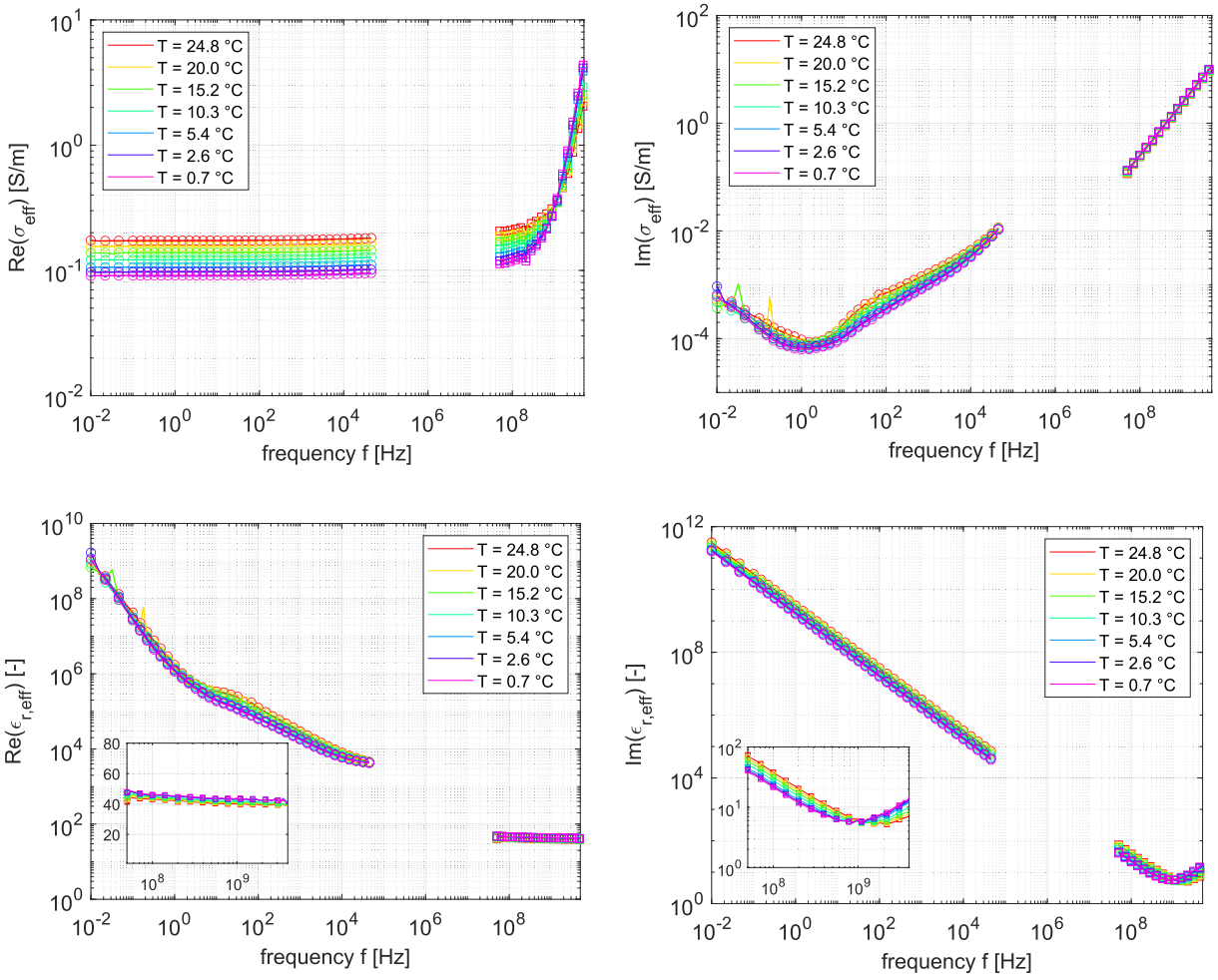

Fig. 4. Ultrabroadband measured spectrums of illite-chlorite, complex conductivity (top, left : real part, right. imaginary part) or complex permittivity (bottom, left. real part, right. imaginary part). LF data with circle marker, HF data with square marker.

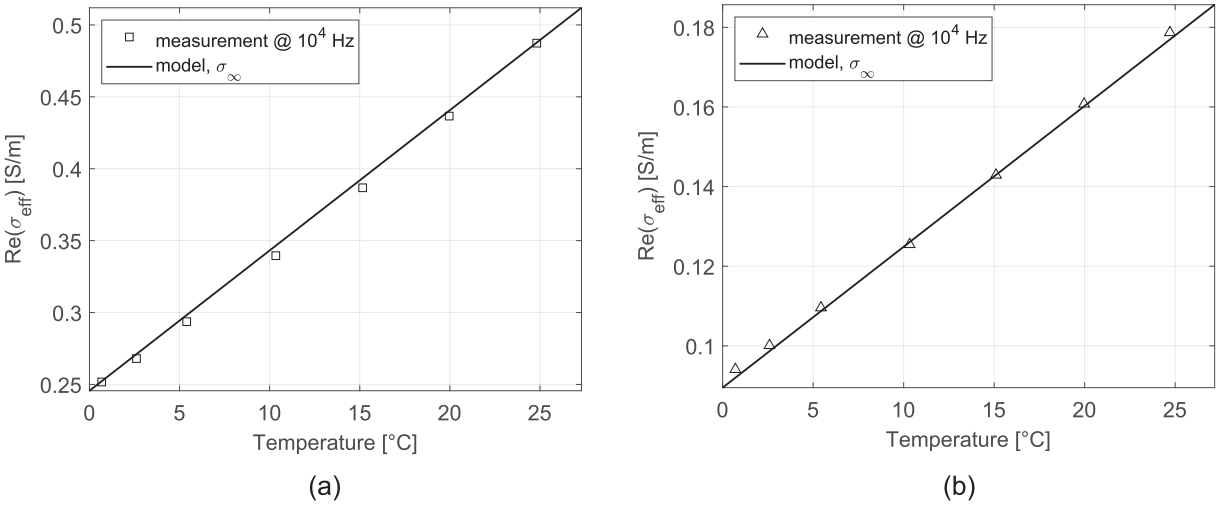

Fig. 5. High frequency conductivity σ_∞ as a function of temperature for a) Montmorillonite sample - b) illite-chlorite sample. Experimental data at $f = 10^4 Hz$.

conductivity.

A broadband modeling framework based on a mixture concept introduced in [28] was presented. The key feature of our approach is that the same formation factor is used to compute the LF and HF contributions. Based on this new approach, the temperature dependency of specific material parameters frequently used in geotechnical and geo-environmental applications were modeled, i.e. real high frequency electrical conductivity and real high frequency dielectric permittivity. A reasonable agreement between measured and modeled results was observed for both clays.

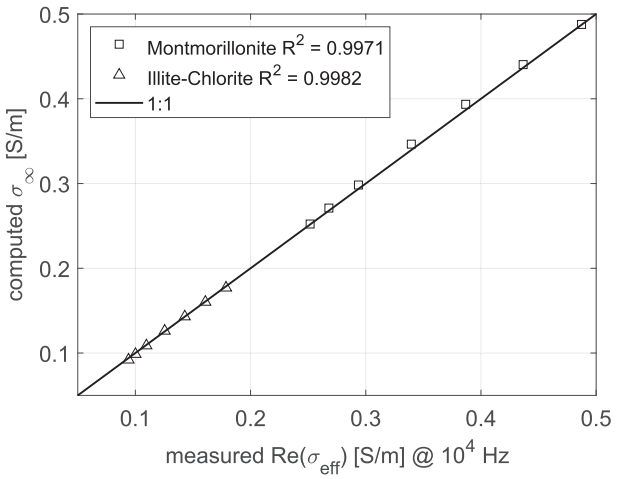

Fig. 6. Computed values of σ_∞ versus measured values at $f = 10^4 Hz$ for both sample for all measurements.

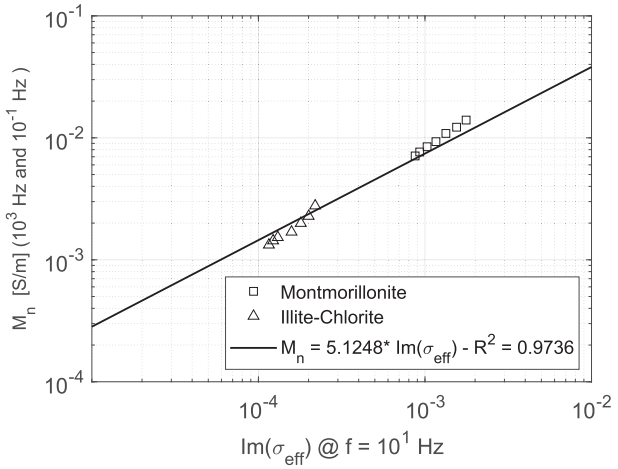

Fig. 7. Comparison between the normalized chargeability (defined as the difference between the in-phase conductivity at $f = 10^3 Hz$ and $f = 10^{-1} Hz$) and the quadrature conductivity at the geometric mean frequency ($f = 10^1 Hz$).

The proposed framework, ultrabroadband measurement in combination with the mixture approach, has a high potential for the geophysical characterization of geomaterials in geotechnical and geo-environmental applications. It enables a combined interpretation of petrophysical and petrochemical quantities obtained with different classic geophysical methods such as ERT (Electrical Resistivity Tomography), IP (Induced Polarization), TDR (Time Domain Reflectometry) and GPR (Ground Penetrating Radar) based on specific electrical material properties.

In further investigations, two electrode impedance measurement will be included to fill the intermediate frequency gap (45 kHz – 50 MHz). The suggested broadband mixture model will be further developed to consider additional interfacial relaxation processes. Our ultimate goal being the development of ultra-broadband pure mechanistic approach in order to develop multi-parameter estimation scheme applicable on the field with typical classic geophysics methods.

Funding

This work was funded by Australian Research Council fellowships awarded to T. Bore (DE180101441) and to A Scheuermann (FT180100692). A. Revil thanks the French National Research Agency (ANR) through the HYDROGEODAM project (ANR-17-CE06–0016). We

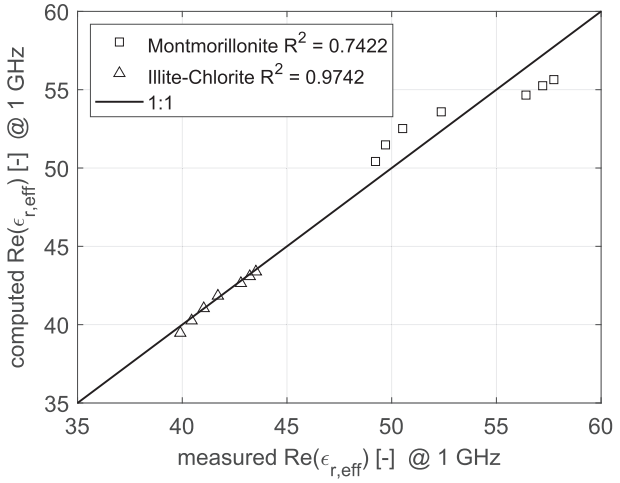

Fig. 9. Computed values versus measured values of $Re(\varepsilon_{r,eff})$ values at $f = 10^9 Hz$ for both sample for all measurements.

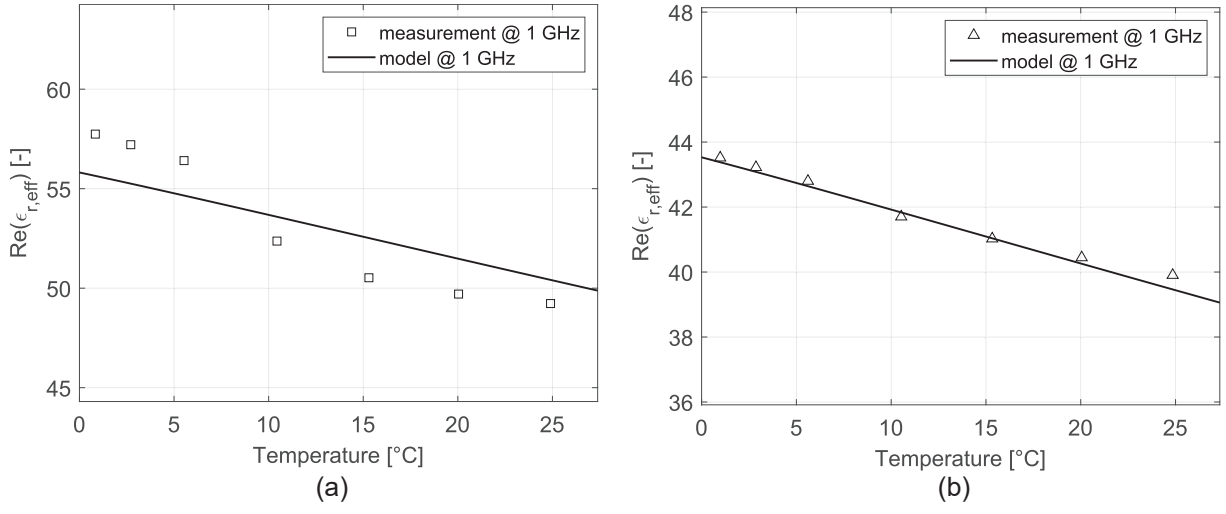

Fig. 8. Real part of relative effective complex permittivity as a function of temperature at 1 GHz for a) Montmorillonite sample - b) illite-chlorite sample.

also thank I-RISK (Research, Development and Innovation platform), the region Auvergne Rhône Alpes (France), and the European FEDER fund for their contribution to this study.

CRediT authorship contribution statement

Thierry Bore: Funding acquisition, Conceptualization, Methodology, Investigation, Software, Validation, Formal analysis, Visualization, Writing – original draft, Writing – review & editing. **Antoine Coperey:** Conceptualization, Methodology, Investigation, Software, Validation, Formal analysis, Visualization, Writing – original draft, Writing – review & editing. **Norman Wagner:** Conceptualization, Methodology, Formal analysis, Software, Writing – original draft, Writing – review & editing. **Partha Narayan Mishra:** Visualization, Writing – original draft, Writing – review & editing. **Alexander Scheuermann:** Funding acquisition, Conceptualization, Resources, Writing – original draft, Writing – review & editing. **André Revil:** Funding acquisition, Conceptualization, Resources, Methodology, Investigation, Formal analysis, Visualization, Writing – original draft, Writing – review & editing, Supervision.

Declaration of Competing Interest

The authors declare that they have no known competing financial interests or personal relationships that could have appeared to influence the work reported in this paper.

Acknowledgement

The authors would like to thank Keysight France for the loan of the VNA (E5071C), and Jacques Grangeon and Martine Le Floch from University Savoie Mont-Blanc for technical support.

Appendix A. Supplementary material

Supplementary data to this article can be found online at https://doi.org/10.1016/j.measurement.2021.110653.

References

[1] A. Binley, S.S. Hubbard, J.A. Huisman, A. Revil, D.A. Robinson, K. Singha, L. D. Slater, The emergence of hydrogeophysics for improved understanding of subsurface processes over multiple scales, Water Resour. Res. 51 (6) (2015) 3837–3866.
[2] C. Power, P. Tsourlos, M. Ramasamy, A. Nivorlis, M. Mkandawire, Combined DC resistivity and induced polarization (DC-IP) for mapping the internal composition of a mine waste rock pile in Nova Scotia, Canada, J. Appl. Geophys. 150 (2018) 40–51.
[3] R. Doherty, B. Kulessa, A.S. Ferguson, M.J. Larkin, L.A. Kulakov, R.M. Kalin, A microbial fuel cell in contaminated ground delineated by electrical self-potential and normalized induced polarization data, J Geophys. Res. Biogeosci. 115 (G3) (2010) 1–11.
[4] A. Revil, M. Karaoulis, T. Johnson, A. Kemna, Review: Some low-frequency electrical methods for subsurface characterization and monitoring in hydrogeology. Hydrogeol J. 2012;20(4):617–58.
[5] B. Kulessa, B. Hubbard, G.H. Brown, Time-lapse imaging of subglacial drainage conditions using three-dimensional inversion of borehole electrical resistivity data, J Glaciol. 52 (176) (2006) 49–57.
[6] A. Kemna, A. Binley, G. Cassiani, E. Niederleithinger, A. Revil, L. Slater, K. H. Williams, A.F. Orozco, F.-H. Haegel, A. Hördt, S. Kruschwitz, V. Leroux, K. Titov, E. Zimmermann, An overview of the spectral induced polarization method for near-surface applications, Near Surf. Geophys. 10 (6) (2012) 453–468.
[7] S. Lambot, E.C. Slob, I. van den Bosch, B. Stockbroeckx, M. Vanclooster, Modeling of ground-penetrating radar for accurate characterization of subsurface electric properties, IEEE Trans. Geosci. Remote Sens. 42 (11) (2004) 2555–2568.
[8] Y.H. Kerr, P. Waldteufel, P. Richaume, J.P. Wigneron, P. Ferrazzoli, A. Mahmoodi, A. Al Bitar, F. Cabot, C. Gruhier, S.E. Juglea, D. Leroux, A. Mialon, S. Delwart, The SMOS Soil Moisture Retrieval Algorithm, IEEE Trans. Geosci. Remote Sensing 50 (5) (2012) 1384–1403.
[9] H. Vanhala, H. Soininen, Laboratory technique for measurement of spectral induced polarization response of soil sampies, Geophys. Prospect. 43 (5) (1995) 655–676.
[10] P.B. Ishai, M.S. Talary, A. Caduff, E. Levy, Y. Feldman, Electrode polarization in dielectric measurements: a review, Meas. Sci. Technol. [Internet]. 24 (10) (2013) 102001, https://doi.org/10.1088/0957-0233/24/10/102001.
[11] A. Kirichek, C. Chassagne, R. Ghose, Predicting the dielectric response of saturated sandstones using a 2-electrode measuring system, Front Phys. 6 (JAN) (2019).
[12] A. Revil, A. Binley, L. Mejus, P. Kessouri, Predicting permeability from the characteristic relaxation time and intrinsic formation factor of complex conductivity spectra, Water Resour Res. 51 (8) (2015) 6672–6700.
[13] A. Weller, L. Slater, Permeability estimation from induced polarization: an evaluation of geophysical length scales using an effective hydraulic radius concept, Near Surf. Geophys. 17 (6) (2019) 581–594.
[14] A. Revil, K. Koch, K. Holliger, Is it the grain size or the characteristic pore size that controls the induced polarization relaxation time of clean sands and sandstones? Water Resour. Res. 48 (5) (2012) 1–7.
[15] A. Revil, M.L. Breton, Q. Niu, E. Wallin, E. Haskins, D.M. Thomas, Induced polarization of volcanic rocks. 2. Influence of pore size and permeability, Geophys. J. Int. 208 (2) (2017) 814–825.
[16] L.B.M. Silva, E.J.P. Santos, Extraction of permittivity and permeability of low-loss fluids taking into account the impedance-mismatch and calibration reference-plane position. Measurement [Internet]. 2014;53:128–35. Available from: http://linkinghub.elsevier.com/retrieve/pii/S0263224114001420.
[17] T. Bore, D. Placko, F. Taillade, P. Sabouroux, Electromagnetic characterization of grouting materials of bridge post tensioned ducts for NDT using capacitive probe, NDT E Int. 60 (2013) 110–120.
[18] T. Bore, H. Bhuyan, T. Bittner, V. Murgan, N. Wagner, A. Scheuermann, A large coaxial reflection cell for broadband dielectric characterization of coarse grained materials, Meas. Sci. Technol. 29 (1) (2018) 015602, https://doi.org/10.1088/1361-6501/aa9407.
[19] R.M. Irastorza, M. Mayosky, F. Vericat, Noninvasive measurement of dielectric properties in layered structure: A system identification approach, Measurement 42 (2) (2009) 214–224.
[20] A. Szypłowska, M. Kafarski, A. Wilczek, A. Lewandowski, W. Skierucha, Salinity index determination of porous materials using open-ended probes, Meas. Sci. Technol. [Internet]. 28 (1) (2017) 014006, https://doi.org/10.1088/1361-6501/28/1/014006.
[21] G.C. Topp, J.L. Davis, A.P. Annan, Electromagnetic Determination of Soil Water Content: Water Resour Res. 16 (3) (1980) 574–582.
[22] S.U. Susha Lekshmi, D.N. Singh, B.M. Shojaei, A critical review of soil moisture measurement, Available from, Measurement [Internet]. 54 (2014) 92–105, http://www.sciencedirect.com/science/article/pii/S0263224114001651.
[23] G. Yan, T. Bore, Z. Li, S. Schlaeger, A. Scheuermann, L. Li, Application of spatial time domain reflectometry for investigating moisture content dynamics in unsaturated loamy sand for gravitational drainage, Appl Sci. 11 (7) (2021) 2994, https://doi.org/10.3390/app11072994.
[24] M. Dobson, F. Ulaby, M. Hallikainen, M. El-rayes, Microwave Dielectric Behavior of Wet Soil-Part II: Dielectric Mixing Models, IEEE Trans. Geosci. Remote Sens. GE-23 (1) (1985) 35–46.
[25] N. Wagner, K. Emmerich, F. Bonitz, K. Kupfer, Experimental investigations on the frequency- and temperature-dependent dielectric material properties of soil, IEEE Trans. Geosci. Remote Sens. 49 (7) (2011) 2518–2530.
[26] T. Bore, N. Wagner, S. Delepine Lesoille, F. Taillade, G. Six, F. Daout, D. Placko, Error analysis of clay-rock water content estimation with broadband high-frequency electromagnetic sensors - air gap effect, Sensors (Switzerland) 16 (4) (2016) 554, https://doi.org/10.3390/s16040554.
[27] T. Bore, N. Wagner, C. Cai, A. Scheuermann, Broadband electromagnetic analysis of compacted kaolin. Meas Sci Technol [Internet]. 2017;28(1):014016. Available from: http://stacks.iop.org/0957-0233/28/i=1/a=014016?key=crossref.8f49b7cefb3af2bf7844b38fa170f7f5.
[28] G.R. Olhoeft, J.R. Banavar, J. Klopik, K.W. Winkler, Electrical properties from 10–3 to 10+ 9 HZ−− Physics and chemistry, AIP Conf Proc. 154 (1) (1987) 281–298.
[29] K. Klein, J.C. Santamarina, Methods for Broad-Band Dielectric Permittivity Measurements (Soil-Water Mixtures, 5 Hz to 1.3 GHz), Geotech. Test J. 20 (2) (1997) 168–178.
[30] A. Cadène, B. Rotenberg, S. Durand-Vidal, J.-C. Badot, P. Turq, Dielectric spectroscopy as a probe for dynamic properties of compacted smectites, Phys. Chem. Earth. 31 (10-14) (2006) 505–510.
[31] X. Dong, Y.-H. Wang, A broadband dielectric measurement technique: theory, experimental verification, and application, J Environ. Eng. Geophys. 14 (1) (2009) 25–38.
[32] P.P. Bobrov, A.V. Repin, O.V. Rodionova, Wideband Frequency Domain Method of Soil Dielectric Property Measurements, Geosci. Remote Sensing, IEEE Trans. 53 (5) (2015) 2366–2372.
[33] T. Ishida, T. Makino, C. Wang, Dielectric-relaxation spectroscopy of kaolinite, montmorillonite, allophane, and imogolite under moist conditions, Clays Clay Miner. 33 (3) (2000) 237–243.
[34] E. Zimmermann, A. Kemna, J. Berwix, W. Glaas, H.M. Münch, J.A. Huisman, A high-accuracy impedance spectrometer for measuring sediments with low polarizability, Meas. Sci. Technol. 19 (10) (2008) 105603, https://doi.org/10.1088/0957-0233/19/10/105603.
[35] M. Loewer, T. Günther, J. Igel, S. Kruschwitz, T. Martin, N. Wagner, Ultra-broadband electrical spectroscopy of soils and sediments-a combined permittivity and conductivity model, Geophys. J. Int. 210 (3) (2017) 1360–1373.
[36] A. Revil, Effective conductivity and permittivity of unsaturated porous materials in the frequency range 1 mHz-1GHz, Water Resour. Res. 49 (1) (2013) 306–327.
[37] Schön JH. Physical properties of rocks: Fundamentals and principles of petrophysics. Elsevier, editor. 2015.
[38] N. Linde, A. Binley, A. Tryggvason, L.B. Pedersen, A. Revil, Improved hydrogeophysical characterization using joint inversion of cross-hole electrical

resistance and ground-penetrating radar traveltime data, Water Resour. Res. 42 (12) (2006) 1–16.
[39] T. Bore, M. Schwing, M. Llano Serna, J. Speer, A. Scheuermann, N. Wagner, A New Broadband Dielectric Model for Simultaneous Determination of Water Saturation and Porosity, IEEE Trans. Geosci. Remote Sens. 56 (8) (2018) 4702–4713.
[40] G.E. Archie, The Electrical Resistivity Log as an Aid in Determining Some Reservoir Characteristics, Available from, Trans AIME [Internet]. 146 (01) (1942) 54–62, http://www.onepetro.org/doi/10.2118/942054-G.
[41] P. Debye, Zur Theorie der spezifischen Wärmen, Ann. Phys. 344 (14) (1912) 789–839.
[42] R. Buchner, J. Barthel, J. Stauber, The dielectric relaxation of water between 0°C and 35°C, Available from, Chem. Phys. Lett. [Internet]. 306 (1–2) (1999) 57–63, http://www.sciencedirect.com/science/article/pii/S0009261499004558.
[43] U. Kaatze, Reference liquids for the calibration of dielectric sensors and measurement instruments, Available from, Meas. Sci. Technol. Meas. Sci. Technol. [Internet]. 18 (18) (2007) 967–976, http://iopscience.iop.org/0957-0233/18/4/002.
[44] A. Revil, N. Florsch, Determination of permeability from spectral induced polarization in granular media, Geophys. J. Int. 181 (3) (2010) 1480–1498.
[45] A. Kirichek, C. Chassagne, R. Ghose, Dielectric spectroscopy of granular material in an electrolyte solution of any ionic strength, Colloids Surf., A 533 (2017) 356–370.
[46] Y. Chen, D. Or, Geometrical factors and interfacial processes affecting complex dielectric permittivity of partially saturated porous media, Water Resour. Res. 42 (6) (2006) 1–9.
[47] S. Arcone, G. Boitnott, Maxwell-Wagner relaxation in common minerals and a desert soil at low water contents [cited 2016 Jun 15]; Available from: J. Appl. Geophys. [Internet]. (2012) http://www.sciencedirect.com/science/article/pii/S0926985111001972.
[48] A. Lorek, N. Wagner, Supercooled interfacial water in fine-grained soils probed by dielectric spectroscopy, Cryosphere. 7 (6) (2013) 1839–1855.
[49] D. Or, J.M. Wraith, Temperature effects on soil bulk dielectric permittivity measured by time domain reflectometry: A physical model, Available from, Water Resour. Res. [Internet]. 35 (2) (1999) 371–383, http://www.scopus.com/scopus/inward/record.url?eid=2-s2.0-0032893450&partnerID=40&rel=R7.0.0.
[50] N. Wagner, T. Bore, J.-C. Robinet, D. Coelho, F. Taillade, S. Delepine-Lesoille, Dielectric relaxation behavior of Callovo-Oxfordian clay rock: A hydraulic-mechanical-electromagnetic coupling approach: DIELECTRIC RELAXATION BEHAVIOR OF COX, J. Geophys. Res. Solid Earth 118 (9) (2013) 4729–4744.
[51] N. Wagner, A. Scheuermann, On the relationship between matric potential and dielectric properties of organic free soils: a sensitivity study, Can Geotech. J. 46 (10) (2009) 1202–1215.
[52] S. Gekle, R.R. Netz, Anisotropy in the dielectric spectrum of hydration water and its relation to water dynamics, J. Chem. Phys. [Internet]. 137 (10) (2012) 104704, https://doi.org/10.1063/1.4749380.
[53] C. Qi, Z. Zhu, C. Wang, Y. Zheng, Anomalously Low Dielectric Constant of Ordered Interfacial Water, J. Phys. Chem. Lett. 12 (2) (2021) 931–937.
[54] T. Bore, P.N. Mishra, N. Wagner, M. Schwing, T. Honorio, A. Revil, A. Scheuermann, Coupled hydraulic, mechanical and dielectric investigations on kaolin, Eng. Geol. 294 (2021) 106352, https://doi.org/10.1016/j.enggeo.2021.106352.
[55] T. Bore, P.N. Mishra, K. Bialkowski, S. Grieve, N. Wagner, A. Scheuermann, Multiple open ended probe for spatio-temporal dielectric spectroscopy: Application to evaporative dewatering. Meas. J. Int. Meas. Confed [Internet]. 2020;173 (September 2020):108521. Available from: https://doi.org/10.1016/j.measurement.2020.108521.
[56] A. Revil, A. Coperey, Z. Shao, N. Florsch, I.L. Fabricius, Y. Deng, J.R. Delsman, P. S. Pauw, M. Karaoulis, P.G.B. de Louw, E.S. van Baaren, W. Dabekaussen, A. Menkovic, J.L. Gunnink, Complex conductivity of soils, Water Resour. Res. 53 (8) (2017) 7121–7147.
[57] T. Bore, N. Wagner, S. Delepine-Lesoille, F. Taillade, G. Six, F. Daout, et al., 3D-FEM modeling of F/TDR sensors for clay-rock water content measurement in combination with broadband dielectric spectroscopy, SAS 2015–2015 IEEE Sensors Appl Symp Proc. (2015).
[58] W.F. Woodruff, A. Revil, C. Torres-Verdín, Laboratory determination of the complex conductivity tensor of unconventional anisotropic shales, Geophysics 79 (5) (2014) E183–E200.
[59] D. Aran, A. Maul, J.-F. Masfaraud, A spectrophotometric measurement of soil cation exchange capacity based on cobaltihexamine chloride absorbance, Comptes Rendus - Geosci. 340 (12) (2008) 865–871.
[60] T. Tartrat, A. Revil, F. Abdulsamad, A. Ghorbani, D. Jougnot, A. Coperey, B. Yven, R. de la Vaissière, Induced polarization response of porous media with metallic particles — Part 10: Influence of desiccation, Geophysics 84 (5) (2019) E357–E375.
[61] A. Coperey, A. Revil, F. Abdulsamad, B. Stutz, P.A. Duvillard, L. Ravanel, Low-Frequency Induced Polarization of Porous Media Undergoing Freezing: Preliminary Observations and Modeling, J. Geophys. Res. Solid Earth. 124 (5) (2019) 4523–4544.
[62] P. Leroy, M. Weigand, G. Mériguet, E. Zimmermann, C. Tournassat, F. Fagerlund, A. Kemna, J.A. Huisman, Spectral induced polarization of Na-montmorillonite dispersions, J. Colloid Interface Sci. 505 (2017) 1093–1110.
[63] F. Abdulsamad, A. Revil, A. Ghorbani, V. Toy, M. Kirilova, A. Coperey, P. A. Duvillard, G. Ménard, L. Ravanel, Complex Conductivity of Graphitic Schists and Sandstones, J. Geophys. Res Solid Earth. 124 (8) (2019) 8223–8249.
[64] Y. Deng, X. Shi, A. Revil, J. Wu, A. Ghorbani, Complex conductivity of oil-contaminated clayey soils, J. Hydrol. 561 (2018) 930–942.
[65] N. Wagner, M. Schwing, A. Scheuermann, Numerical 3-D FEM and Experimental Analysis of the Open-Ended Coaxial Line Technique for Microwave Dielectric Spectroscopy on Soil, IEEE Trans. Geosci. Remote Sens. [Internet]. 52 (2) (2014) 880–893. Feb [cited 2016 Jun 14, http://ieeexplore.ieee.org/lpdocs/epic03/wrapper.htm?arnumber=6484935.
[66] A.P. Gregory, R.N. Clarke, Tables of the Complex Permittivity of Dielectric Reference Liquids at Frequencies up to 5 GHz; NPL Report MAT 23. Innovation. 2009;(March):1–87.
[67] P.N. Mishra, T. Bore, Y. Jiang, A. Scheuermann, L. Li, Dielectric spectroscopy measurements on kaolin suspensions for sediment concentration monitoring, Measurement 121 (January) (2018) 160–169.
[68] P.N. Mishra, T. Bore, A. Scheuermann, L. Li, Measurement of dielectric properties of Kaolin with saline pore fluid during dewatering. In: Proceedings of the 19th International Conference on Soil Mechanics and Geotechnical Engineering, Seoul, 2017.